

Global magnetic phase diagram and multiple unconventional magnets in NiAs-type compounds

Shibo Shen^{1,2,3} and Yilin Wang^{1,2,3,*}

¹*School of Emerging Technology, University of Science and Technology of China, Hefei 230026, China*

²*Hefei National Laboratory, Hefei 230088, China*

³*New Cornerstone Science Laboratory, University of Science and Technology of China, Hefei, 230026, China*

(Dated: May 28, 2026)

NiAs-type compounds such as CrSb and MnTe host g -wave altermagnet (AM) state. In order to search other possible unconventional magnets in this system, we present a global magnetic phase diagram based on a classical J_1 - J_2 - J_3 Heisenberg model and density functional theory (DFT) calculations. We find another g -wave AM state and two f -wave OPMs in the phase diagram. Intriguingly, we show that a mixed-parity of the f -wave OPM and g -wave AM state can naturally emerge in an umbrella-like noncollinear magnetic structure. Our DFT calculations show that CrSe and CrTe_{1-x}Se_x are generally in such mixing state with dominated f -wave component. The interlayer next-nearest-neighbor coupling J_3 is shown to be crucial in determining the phase diagram and in inducing strong competition between conventional and unconventional magnets. Inspired by this, we demonstrate that AM or OPM could be realized by applying chemical doping or strain to conventional magnets. Our results provide a guidance for design of both even- and odd-parity as well as mixed-parity unconventional magnets in NiAs-type compounds.

Introduction. The discovery of altermagnet (AM) has drawn extensively attention to the unconventional anti-ferromagnets (AFM) with non-relativistic spin-splitting in momentum space but without net magnetization [1–13], due to potential applications, such as spintronics [14–19], multifunctional materials [20–22], and unconventional superconductivity [23–31]. The spin space group is the tool for describing such states [32–40]. According to the parity of the spin textures in momentum space, they are generally classified into even-parity [$\mathbf{s}(\mathbf{k}) = \mathbf{s}(-\mathbf{k})$, d, g, i -wave] and odd-parity [$\mathbf{s}(\mathbf{k}) = -\mathbf{s}(-\mathbf{k})$, p, f, h -wave]. Altermagnet belongs to even-parity with broken time reversal T but preserved spatial inversion P in band structures, and its zero magnetization is guaranteed by real-space rotational transformation rather than by translation or inversion. Many altermagnet candidates have been proposed, such as d -wave RuO₂ [41–47], AV₂Se₂O family [4, 48–54], g -wave CrSb [55–59] and MnTe [60–65], just to name a few. Odd-parity magnets (OPM), in contrast, with preserved T but broken P in band structures, are also proposed [66–68]. They exhibit various properties such as transport anisotropy [66, 69], Edelstein effect [70, 71] and unconventional superconductivity [72–78]. Materials such as CeNiAsO [66, 68, 79], Mn₃GaN [66], NiI₂ [80], Gd₃(Ru_{1- δ} Rh _{δ})₄Al₁₂ [81], Fe-based superconductors [79, 82] have been predicted. However, the direct observation of spin splitting in these OPMs by experiments such as ARPES have not been reported, probably due to the complexity of these materials. Thus, more OPM candidates, especially those with quasi-two-dimensional and metallic nature, need to be designed theoretically.

The widely studied g -wave AM CrSb and MnTe belong to the family of NiAs-type compounds. This system features nonsymmorphic space group (P6₃/mmc) and tri-

angular magnetic sublattice. The inversion operator is usually nontrivial in the nonsymmorphic space group [79] and the frustration of triangular lattice usually results in noncollinear (NCL) magnetic structure which are both crucial for realizing OPM [31, 39, 83–85]. This indicates that the NiAs-type compounds should be also a good platform for hosting OPMs. However, a global magnetic phase diagram guiding the search and design of these unconventional magnets in this system is not yet available. A more interesting question is whether a mixed-parity of the AM and OPM magnets could naturally realize or not in this system.

In this paper, in order to search other possible unconventional magnets, in particular, OPMs in NiAs-type compounds, we present a global magnetic phase diagram based on a classical J_1 - J_2 - J_3 Heisenberg model and density functional theory (DFT) calculations. We find two g -wave AMs and two f -wave OPMs in this system. Intriguingly, we demonstrate that an umbrella-like NCL magnetic structure [86, 87] is actually a parity-mixing of f -wave OPM and g -wave AM state. Our DFT calculations show that CrSe and CrTe_{1-x}Se_x are generally in such mixing state with dominated f -wave component. We show the important roles of the interlayer next-nearest-neighbor coupling J_3 in inducing strong competition between conventional and unconventional magnets. Inspired by this, we show that AM and OPM could be realized by applying chemical doping or strain to conventional FM or AFM states. We thus provide a feasible route for search and design of both even- and odd-parity as well as mixed-parity unconventional magnets in the NiAs-type compounds.

Phase diagram of classical J_1 - J_2 - J_3 model. We begin the analysis of the possible magnetic states in NiAs-type compounds based on a minimal classical J_1 - J_2 - J_3

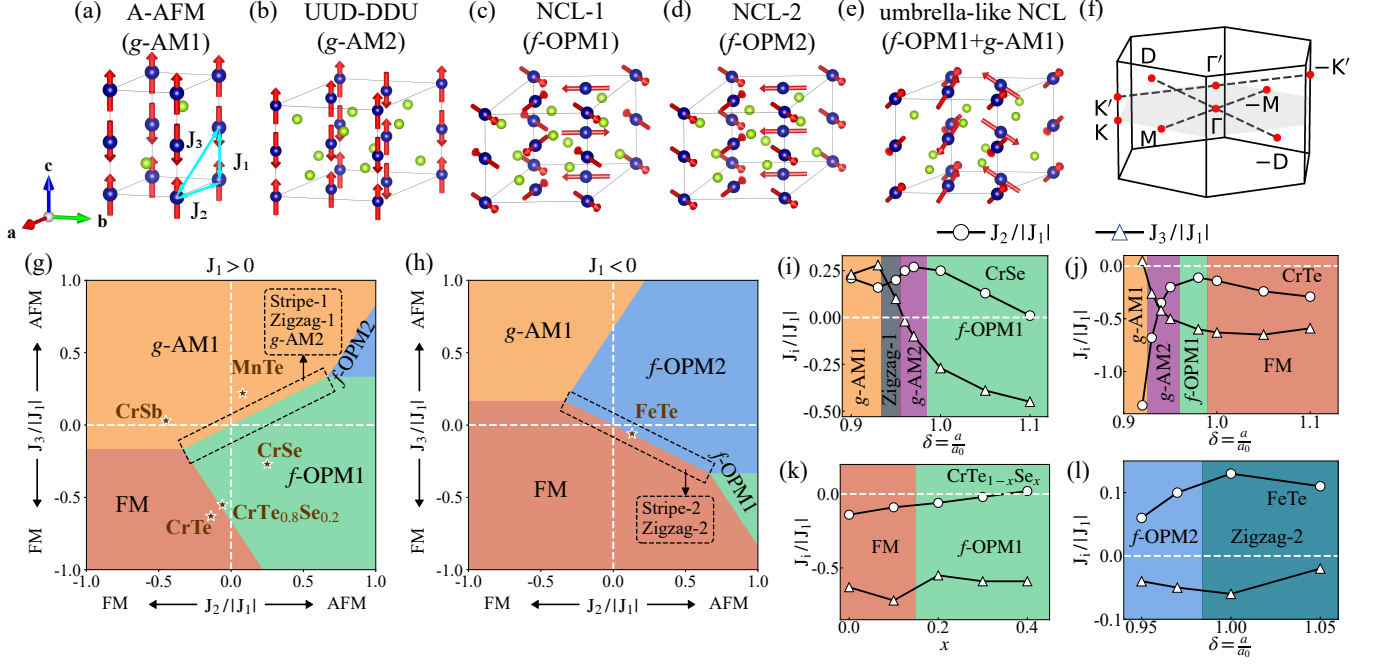


FIG. 1. (a)-(e) Five unconventional magnetic structures. (f) Brillouin zone and k -path for plotting band structures. (g) and (h) $J_2/|J_1| - J_3/|J_1|$ phase diagrams of the J_1 - J_2 - J_3 model for AFM and FM coupling of J_1 , respectively. (i)-(l) DFT calculated $J_2/|J_1|$, $J_3/|J_1|$ and ground state of CrSe, CrTe, $\text{CrTe}_{1-x}\text{Se}_x$ and FeTe as functions of lattice parameters a or chemical compositions. $J_1 > 0$ in CrSe, CrTe and $\text{CrTe}_{1-x}\text{Se}_x$, while $J_1 < 0$ in FeTe. Note that CrSe and $\text{CrTe}_{0.8}\text{Se}_{0.2}$ are generally in the umbrella-like mixed-parity state, with a very small component of g -AM1 in addition to the dominated f -OPM1 component.

Heisenberg model. As shown in Fig. 1(a), J_1 and J_3 are the interlayer nearest-neighbors (NN) and next-nearest-neighbors (NNN) couplings, respectively, and J_2 is the intralayer NN coupling. We use the convention that $J_i > 0$ ($J_i < 0$) for AFM (FM) coupling. Besides FM state, five unconventional AFM states could exist in the $1 \times 1 \times 1$ or $\sqrt{3} \times \sqrt{3} \times 1$ supercell. As shown in Fig. 1, they are (a) collinear A-type AFM; (b) UUD-DDU, intralayer collinear AFM order with two spin up and one spin down, and with interlayer AFM order; (c) NCL-1, coplanar 120° -noncollinear AFM order and interlayer AFM order, (d) NCL-2, analogous to NCL-1 but with interlayer FM order. Generally, canted moments along the c -axis in NCL-1 could be possible, which leads to a noncoplanar umbrella-like NCL state, as shown in Fig. 1(e). We also consider conventional collinear stripe and zigzag AFM states that may also occur in triangular lattices [88], in $2 \times 1 \times 1$ and $2 \times 3 \times 1$ supercells (we term Stripe-1/Zigzag-1 and Stripe-2/Zigzag-2 for interlayer AFM and FM orders, respectively. See Supplementary Materials [89]).

The A-type AFM is the extensively studied g -wave altermagnet in CrSb and MnTe, and the UUD-DDU is also a g -wave altermagnet identified by the online tool *FIND-SPINGROUP* [90], so we label them as g -AM1 and g -AM2, respectively. We find that the spin space group of NCL-1 and NCL-2 do not contain the combined symme-

try PT or multiple spin-rotation-translation symmetries with distinct rotation axes, but contain symmetry operations like $\{U_z(\theta)||I|\tau\}$ and $\{TU_z(\pi)||I\}$, where $U_z(\theta)$ is spin rotation around z -axis, τ is a spatial fractional translation, and I is spatial identity. According to the symmetry criteria [39, 40], NCL-1 and NCL-2 are OPMs with a f -wave spin-texture ($s_z(\mathbf{k}) = -s_z(-\mathbf{k})$, $s_{x,y}(\mathbf{k}) = 0$). We label them as f -OPM1 and f -OPM2, respectively. In the umbrella-like NCL structure, the symmetry $\{TU_z(\pi)||I\}$ is broken and there are no other symmetries satisfying the condition for OPM due to the additional out-of-plane moments. However, these out-of-plane components actually form a A-AFM structure (g -AM1 state), so this umbrella-like state is a parity-mixing of f -OPM1 and g -AM1 states. Since both states have nonzero spin-texture of only $s_z(\mathbf{k})$, its spin-texture is a mixing of f - and g -waves of $s_z(\mathbf{k})$.

The total energies derived from this classical J_1 - J_2 - J_3 model are (per $1 \times 1 \times 1$ cell, assuming $|\vec{S}_i| = 1$),

$$E_{g\text{-AM1}} = -2J_1 + 6J_2 - 12J_3, \quad (1)$$

$$E_{g\text{-AM2/Stripe-1/Zigzag-1}} = -2J_1 - 2J_2 + 4J_3, \quad (2)$$

$$E_{f\text{-OPM1}} = -2J_1 - 3J_2 + 6J_3, \quad (3)$$

$$E_{f\text{-OPM2}} = 2J_1 - 3J_2 - 6J_3, \quad (4)$$

$$E_{\text{FM}} = 2J_1 + 6J_2 + 12J_3, \quad (5)$$

$$E_{\text{Stripe-2/Zigzag-2}} = 2J_1 - 2J_2 - 4J_3. \quad (6)$$

TABLE I. The DFT calculated magnetic exchange couplings ($|\vec{S}_i| = 1$, meV) and total energies (per the $1 \times 1 \times 1$ cell, meV) of nine magnetic states, for several NiAs-type materials. The numbers in the parenthesis are the total energies calculated by Eqns. 1-6 with the calculated J_i as inputs.

Material	J_1	J_2	J_3	g -AM1	g -AM2	f -OPM1	f -OPM2	FM	Stripe-1	Stripe-2	Zigzag-1	Zigzag-2
CrSb	74.9	-34.0	2.2	0(0)	325 (307)	350 (346)	635 (619)	350 (352)	307 (307)	588 (589)	313 (307)	578 (589)
MnTe	42.0	3.2	9.2	0(0)	132 (122)	154 (137)	213 (194)	387 (389)	120 (122)	216 (216)	118 (122)	212 (216)
CrSe	30.3	7.7	-8.1	250(215)	18 (24)	0 (0)	256 (218)	177 (142)	58 (24)	239 (210)	30 (24)	235 (210)
CrTe _{0.8} Se _{0.2}	27.0	-1.7	-14.9	251(253)	18 (28)	0 (0)	232 (287)	6 (3)	39 (28)	213 (255)	26 (28)	199 (255)
CrTe	21.0	-3.0	-13.2	189(233)	18 (46)	7 (22)	197 (265)	0 (0)	31 (46)	188 (235)	25 (46)	178 (235)
FeTe	-95.4	12.3	-5.4	358(525)	198 (340)	145 (317)	3 (0)	36 (14)	280 (340)	25 (2)	228 (340)	0 (2)
FeTe(0.97a ₀)	-74.8	7.3	-4.1	415(398)	244 (274)	186 (258)	0 (8)	17 (0)	291 (274)	24 (7)	280 (274)	5 (7)

For the parity-mixing state of f -OPM1 + g -AM1, the energy is $-2J_1 - (3J_2 - 6J_3)(\cos^2\theta - 2\sin^2\theta)$, where θ is the canted angle between the magnetic moment and ab -plane. It cannot be ground state under this classical and isotropic approximation since $\cos^2\theta - 2\sin^2\theta$ is a monotonic decreasing function when $\theta \in [0, \pi/2]$ (either f -OPM1 or g -AM1 as ground state). Quantum fluctuations or anisotropic exchange couplings may induce a certain degree of mixing [85], as confirmed by our DFT calculation.

We plot a $J_2/|J_1| - J_3/|J_1|$ phase diagram for the magnetic ground state of this model in Fig. 1(g) and (h) for AFM and FM J_1 coupling, respectively. When $J_3 = 0$, the magnetic ground state is independently determined by the interlayer and intralayer NN couplings, so there are four different ground states: (i) f -OPM1 when $J_1 > 0$ and $J_2 > 0$; (ii) g -AM1 when $J_1 > 0$ and $J_2 < 0$; (iii) f -OPM2 when $J_1 < 0$ and $J_2 > 0$; (iv) FM when $J_1 < 0$ and $J_2 < 0$. We find that finite J_3 plays important roles in determining the phase diagram although J_3 is smaller than J_1 . This is because the multiplicity of the J_3 couplings are larger than that of J_1 and J_2 . For instance, a FM J_3 coupling could lead to a nontrivial FM ground state even J_1 or J_2 is AFM coupling. Meanwhile, a FM J_3 coupling also tends to stabilize the f -OPM1 state even J_2 or J_1 is FM coupling. This will result in strong competition between FM and f -OPM1 state, as shown in the bottom-left of Fig. 1(g). While, an AFM J_3 coupling will stabilize the g -AM1 state even J_2 is AFM coupling or J_1 is FM coupling, and it will also stabilize the f -OPM2 state even J_1 is AFM coupling or J_2 is FM coupling.

We note that, in this classical J_1 - J_2 - J_3 model, the g -AM2, stripe and zigzag states can only become ground state at the phase boundary $2J_3 = J_2$ ($J_1 > 0$) or $2J_3 = -J_2$ ($J_1 < 0$), but they are still degenerate with g -AM1 and f -OPM1 at $2J_3 = J_2$ [Fig. 1(g)], or degenerate with f -OPM2 and FM at $2J_3 = -J_2$ [Fig. 1(g)]. Several factors could drive them to be ground state. Firstly, since the effect of J_2 has been canceled out by J_3 , longer intralayer exchange couplings start to play roles. For example, if the intralayer NNN coupling J_4 is considered, Stripe-1 and Zigzag-1 states may become ground state

when $-J_4 < J_2 - 2J_3 < 8J_4$ and $-\frac{2}{3}J_4 < J_2 - 2J_3 < \frac{16}{3}J_4$, respectively, and the Stripe-2 and Zigzag-2 states may become ground states when $-J_4 < J_2 + 2J_3 < 8J_4$ and $-\frac{2}{3}J_4 < J_2 + 2J_3 < \frac{16}{3}J_4$, respectively. Secondly, the symmetry of these AFM states are lower than that of FM, g -AM1, f -OPM1 and f -OPM2, so there will be concomitant lattice distortion that will further reduce energy. Thirdly, quantum fluctuations also play important roles in stabilizing these states. It is expected that the phase boundary of this classical model will be reshaped by these factors, so we roughly indicate these states near the phase boundary ($2J_3 = J_2$ and $2J_3 = -J_2$) by the dashed rectangles in the phase diagram. The existence of these states have been confirmed by our DFT calculations.

NiAs-type materials and phase transition. We perform DFT calculations for several representative NiAs-type compounds including CrSb, MnTe, CrSe, CrTe, CrTe _{x} Se _{$1-x$} and hexagonal FeTe, to verify the model and search more candidates of unconventional magnets. The DFT calculated magnetic exchange couplings J_1 , J_2 , J_3 and the total energies of different magnetic states are shown in Table I. The numbers in the parenthesis are the total energy calculated by Eqns. 1-6 with the calculated J_i as inputs. The ground state and the energy sequence of other magnetic states obtained by the J_1 - J_2 - J_3 model agree well with the DFT results. The only exception is FeTe where the ground state obtained by DFT and the model is slightly different, because it is very close to the phase boundary ($2J_3 = -J_2$).

The calculated J_i is dominated by the interlayer NN coupling J_1 . It is FM coupling for FeTe and AFM coupling for all other compounds. We have reproduced the g -AM1 ground state for CrSb and MnTe [91–96]. We note that, although the calculated J_2 is AFM coupling for MnTe, the AFM J_3 coupling has overcome J_2 to stabilize a g -AM1 ground state, consistent with our model analysis and previous studies [95, 97, 98]. We note that the important roles of J_3 in stabilizing the g -AM1 state in MnTe was also discussed by I. Mazin in Ref. [98].

Our DFT calculations find that the ground state of CrSe is the mixed-parity umbrella-like state, but it is

dominated by the f -OPM1 component. The calculated J_3 (-8.1 meV) is strong FM coupling, which helps to stabilize the f -OPM1 component. The calculated in-plane magnetic moment is about $3 \mu_B$, and the out-of-plane moment is only about $0.1 \mu_B$, which leads to a small canted angle $\theta \sim 2^\circ$. This is consistent with our analysis based on the classical J_1 - J_2 - J_3 model. Since the g -AM1 component is much smaller than the f -OPM1 component, we still term the ground state of CrSe as f -OPM1 in the phase diagram [Fig. 1(g)] and Table I for simplicity. We note that a neutron diffraction experiment performed on CrSe by L.M. Corliss *et al.* in 1961 inferred that it has an umbrella-like NCL magnetic structure with large canted angle $\theta \sim 45^\circ$ [86]. This discrepancy might be caused by sample quality. Studies have shown that there might be other coexisting phases such as Cr₂Se₃, Cr₃Se₄, Cr₅Se₈, Cr₇Se₈ [99–107] when growing the CrSe samples. In particular, a recent study has inferred that there should be Cr₆Se₈ phase in the sample used in the neutron diffraction experiment [108]. This will significantly affect the results and analysis of neutron diffraction experiments. Further experiment with high quality CrSe sample is required to confirm the exact canted angle.

To clearly show that the umbrella-like state is a mixed-parity of $s_z(\mathbf{k})$, we compare band structures and Fermi surfaces of CrSe between a pure f -OPM1 state ($\theta = 0^\circ$) and a hypothetical state with equally mixing of f -OPM1 and g -AM1 ($\theta = 45^\circ$) in Fig. 2. Our calculations confirm $s_{xy}(\mathbf{k}) = 0$ and only $s_z(\mathbf{k})$ are nonzero. The pure f -OPM1 state shows odd-parity f -wave spin splitting in both high-symmetry ($k_z = 0$ plane, $-M$ - Γ - M line) and low-symmetry ($-D$ - Γ - D) plane/lines [Figs. 2(a)-(c)]. The mixed-parity state exhibits only odd-parity f -wave spin splitting induced by the f -OPM1 component in the $k_z = 0$ plane [Figs. 2(d),(f)], since the g -AM1 component does not induce spin splitting in this plane. While, the mixed-parity state induces both even-parity [$s_z(\mathbf{k}) = s_z(-\mathbf{k})$] and odd-parity [$s_z(\mathbf{k}) = -s_z(-\mathbf{k})$] spin splitting along the low-symmetry line $-D$ - Γ - D , so the net result is $s_z(\mathbf{k}) \neq -s_z(-\mathbf{k})$, as shown in Fig. 2(e).

We apply in-plane biaxial strain (changing lattice parameter a , with fixed c) on CrSe to explore possible phase transitions [Fig. 1(i)]. The calculated J_1 and J_2 stay AFM coupling, while J_3 gradually changes from FM coupling to AFM coupling as decreasing a . This drives phase transitions from f -OPM1 to g -AM2 ($0.97a_0$), and then to Zigzag-1 ($0.95a_0$), and finally to g -AM1, because AFM J_3 coupling tends to stabilize the g -AM1 state. We note that $2J_3 \approx J_2$ in the Zigzag-1 state. This confirms the existence of Zigzag-1 and g -AM2 state near the phase boundary between g -AM1 and f -OPM1, consistent with our analysis based on the J_1 - J_2 - J_3 model.

Our DFT calculations find a FM ground state for CrTe, which is consistent with experiments [109, 110]. This FM state is nontrivial since the calculated J_1 (21 meV) is strong AFM coupling. It is still stabilized by the strong

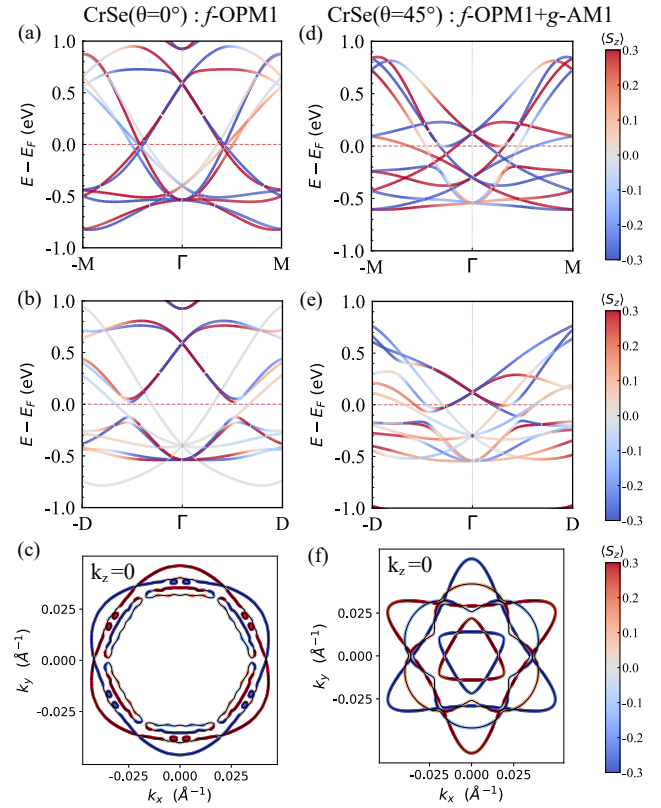


FIG. 2. Band structures of CrSe along (a),(d) high-symmetry line $-M$ - Γ - M and (b),(e) low-symmetry line $-D$ - Γ - D , where the fractional coordinate of D is (0.3, 0.2, 0.2). (c),(f) Fermi surface at $k_z = 0$ plane. (a)-(c) for pure f -OPM1 state ($\theta = 0^\circ$), and (d)-(f) for mixed-parity f -OPM1+ g -AM1 state ($\theta = 45^\circ$). The color indicates the expectation value of $s_z(\mathbf{k})$.

FM J_3 coupling (-13.2 meV) as we discussed above. Meanwhile, AFM J_1 and FM J_3 couplings also favor a f -OPM1 state. This leads to strong competition between the FM ground state and f -OPM1 state in CrTe, so it locates near the phase boundary as shown in the bottom-left of the phase diagram [Fig. 1(g)]. The DFT calculated total energy of the f -OPM1 state is only 7 meV higher than that of the FM state (Table I). Therefore, the relative strength between J_3 and J_1 is the key factor determining either FM or f -OPM1 as ground state. Inspired by this, we replace some Te with Se to drive CrTe into the f -OPM1 state. This is confirmed by our DFT calculations shown in Fig. 1(k), where the ground state of CrTe_{1-x}Se_x becomes f -OPM1 when $x \geq 0.2$. $|J_3/J_1|$ of CrTe_{0.8}Se_{0.2} (0.55) becomes smaller than that of CrTe (0.63) [see Table I and Fig. 1(g)]. The calculated in-plane magnetic moment is about $3.5 \mu_B$. Similar to CrSe, there is also a very small canted moment ($\sim 0.1 \mu_B$) along the c -axis. So, CrTe_{1-x}Se_x is also a mixed-parity state with dominated f -OPM1 component. This is confirmed by the calculated band structure and Fermi

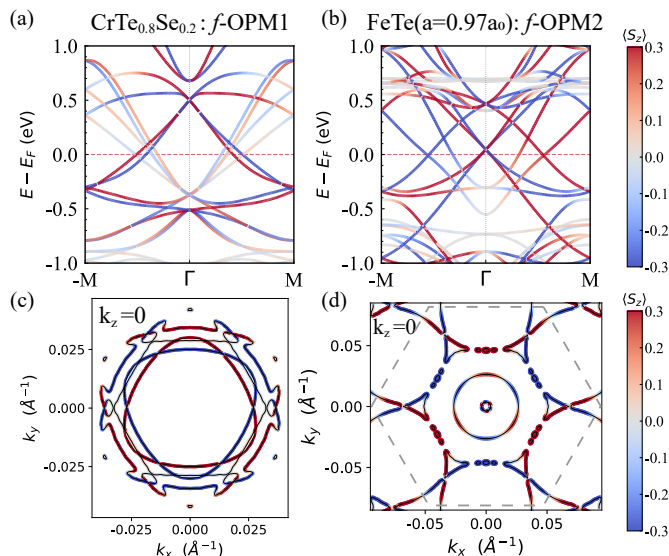


FIG. 3. (a),(b) Band structures along $-M-\Gamma-M$ line. (c),(d) Fermi surface at $k_z = 0$. (a),(c) for $\text{CrTe}_{0.8}\text{Se}_{0.2}$ and (b),(d) for FeTe with in-plane compressive strain ($a = 0.97a_0$). The color indicates the expectation value of $s_z(\mathbf{k})$

surface at $k_z = 0$ which exhibits a f -wave spin splitting of $s_z(\mathbf{k})$ [see Fig. 3(a) and (c)].

We also apply in-plane biaxial strain to explore possible phase transition, which is shown in Fig. 1(j). As decreasing a (with fixed c), J_1 stays AFM coupling; J_3 tends to change from FM coupling to AFM coupling, while J_2 stays FM coupling and its strength first decreases and then significantly increases. This drives successive phase transitions from FM to f -OPM1 ($0.97a_0$), and then to g -AM2 ($0.95a_0$) and g -AM1 ($0.92a_0$). This demonstrates rich phase transitions among the multiple unconventional magnets in NiAs-type compounds.

For hexagonal FeTe , the calculated J_1 (-95.4 meV) and J_3 (-5.4 meV) are both FM coupling, and J_2 (12.3 meV) is AFM coupling. We note that $2J_3 \approx -J_2$, so it is near the phase boundary between FM and f -OPM2. Our DFT calculations find Zigzag-2 as the ground state for FeTe , consistent with our analysis based on the J_1 - J_2 - J_3 model. We find pretty large distortions of the triangular lattice in this state, which further reduces energy such that it becomes ground state. However, its energy is still close to that of f -OPM2 and FM states [see Table. I], indicating strong competition. Indeed, FM state was found in ultrathin film of hexagonal FeTe [111]. We find that in-plane compressive strain could drive it to the f -OPM2 state [see Fig. 1(l)]. For example, at $a = 0.97a_0$, f -OPM2 becomes ground state, with 5 meV lower in energy than that of Zigzag-2 (Table I). The band structure and Fermi surface at $k_z = 0$ show a f -wave spin splitting, as shown in Figs. 3(b) and (d).

Conclusion and discussion. To conclude, we have presented a global magnetic phase diagram for NiAs-type

compounds, and we find multiple unconventional magnets including two g -wave AMs and two f -wave OPMS. A mixed-parity of f - and g -wave magnet could also naturally emerge in an umbrella-like NCL structure in this system. Our DFT calculations show that CrSe and $\text{CrTe}_{1-x}\text{Se}_x$ are generally in such mixed-parity state. The interlayer NNN coupling J_3 is found to be crucial in inducing strong competition between conventional and unconventional magnets. In particular, it could induce a nontrivial FM state even when J_1 is AFM coupling. This leads to strong competition between FM and f -OPM1 states. It also induces competing states near the phase boundary setting by $2J_3 = J_2$ and $2J_3 = -J_2$. Inspired by this, we demonstrate that rich phase transitions and unconventional magnets could be realized by chemical doping or in-plane strain. Our results demonstrate that the NiAs-type compounds is a good platform for realizing both even- and odd-parity as well as mixed-parity unconventional magnets, and the phase diagram provides a guidance for design of such magnets. The predicted unconventional magnets CrSe , $\text{CrTe}_{1-x}\text{Se}_x$ and FeTe are metallic, which are beneficial to construct heterostructure with superconductors for realizing topological superconducting state via proximity effect.

Note added. We note that two recent works posted in arXiv server also discussed the mixed-parity magnets [112, 113]. Ref. [112] terms such states as unconstrained-parity magnet and candidate materials including CrSe are discussed. Ref. [113] proposes using circularly polarized light to drive mixed-parity magnets in collinear magnetic orders.

Acknowledgement. This project was supported by National Key R&D Program of China (Grant No. 2023YFA1406304), the Quantum Science and Technology-National Science and Technology Major Project (No. 2021ZD0302803) and the New Cornerstone Science Foundation. The calculations were performed in Hefei Advanced Computing Center, China.

* yilinwang@ustc.edu.cn

- [1] Y. Noda, K. Ohno, and S. Nakamura, Momentum-dependent band spin splitting in semiconducting MnO_2 : a density functional calculation, *Phys. Chem. Chem. Phys.* **18**, 13294 (2016).
- [2] S. Hayami, Y. Yanagi, and H. Kusunose, Momentum-dependent spin splitting by collinear antiferromagnetic ordering, *Journal of the Physical Society of Japan* **88**, 123702 (2019).
- [3] H.-Y. Ma, M. Hu, N. Li, J. Liu, W. Yao, J.-F. Jia, and J. Liu, Multifunctional antiferromagnetic materials with giant piezomagnetism and noncollinear spin current, *Nature Communications* **12**, 2846 (2021).
- [4] M. Hu, X. Cheng, Z. Huang, and J. Liu, Catalog of c -paired spin-momentum locking in antiferromagnetic systems, *Phys. Rev. X* **15**, 021083 (2025).

- [5] L. Šmejkal, J. Sinova, and T. Jungwirth, Emerging research landscape of altermagnetism, *Phys. Rev. X* **12**, 040501 (2022).
- [6] L. Šmejkal, J. Sinova, and T. Jungwirth, Beyond conventional ferromagnetism and antiferromagnetism: A phase with nonrelativistic spin and crystal rotation symmetry, *Phys. Rev. X* **12**, 031042 (2022).
- [7] L. Šmejkal, A. H. MacDonald, J. Sinova, S. Nakatsuji, and T. Jungwirth, Anomalous hall antiferromagnets, *Nature Reviews Materials* **7**, 482 (2022).
- [8] T. Jungwirth, R. M. Fernandes, J. Sinova, and L. Šmejkal, *Altermagnets and beyond: Nodal magnetically-ordered phases* (2024), arXiv:2409.10034 [cond-mat.mtrl-sci].
- [9] Y. Guo, H. Liu, O. Janson, I. C. Fulga, J. van den Brink, and J. I. Facio, Spin-split collinear antiferromagnets: A large-scale ab-initio study, *Materials Today Physics* **32**, 100991 (2023).
- [10] L. Bai, W. Feng, S. Liu, L. Šmejkal, Y. Mokrousov, and Y. Yao, Altermagnetism: Exploring new frontiers in magnetism and spintronics, *Advanced Functional Materials* **34**, 2409327 (2024).
- [11] P. A. McClarty and J. G. Rau, Landau theory of altermagnetism, *Phys. Rev. Lett.* **132**, 176702 (2024).
- [12] Q. Liu, X. Dai, and S. Blügel, Different facets of unconventional magnetism, *Nature Physics* **21**, 329 (2025).
- [13] H. Zhu, J. Li, X. Chen, Y. Yu, and Q. Liu, Magnetic geometry induced quantum geometry and nonlinear transports, *Nature Communications* **16**, 4882 (2025).
- [14] R. González-Hernández, L. Šmejkal, K. Výborný, Y. Yahagi, J. Sinova, T. c. v. Jungwirth, and J. Železný, Efficient electrical spin splitter based on nonrelativistic collinear antiferromagnetism, *Phys. Rev. Lett.* **126**, 127701 (2021).
- [15] L. Šmejkal, A. B. Hellenes, R. González-Hernández, J. Sinova, and T. Jungwirth, Giant and tunneling magnetoresistance in unconventional collinear antiferromagnets with nonrelativistic spin-momentum coupling, *Phys. Rev. X* **12**, 011028 (2022).
- [16] R.-W. Zhang, C. Cui, R. Li, J. Duan, L. Li, Z.-M. Yu, and Y. Yao, Predictable gate-field control of spin in altermagnets with spin-layer coupling, *Phys. Rev. Lett.* **133**, 056401 (2024).
- [17] L. Han, X. Fu, R. Peng, X. Cheng, J. Dai, L. Liu, Y. Li, Y. Zhang, W. Zhu, H. Bai, Y. Zhou, S. Liang, C. Chen, Q. Wang, X. Chen, L. Yang, Y. Zhang, C. Song, J. Liu, and F. Pan, Electrical 180° switching of néel vector in spin-splitting antiferromagnet, *Science Advances* **10**, eadn0479 (2024).
- [18] Z. Zhou, X. Cheng, M. Hu, R. Chu, H. Bai, L. Han, J. Liu, F. Pan, and C. Song, Manipulation of the altermagnetic order in CrSb via crystal symmetry, *Nature* **638**, 645 (2025).
- [19] Y. Zhang, H. Bai, J. Dai, L. Han, C. Chen, S. Liang, Y. Cao, Y. Zhang, Q. Wang, W. Zhu, F. Pan, and C. Song, Electrical manipulation of spin splitting torque in altermagnetic RuO₂, *Nature Communications* **16**, 5646 (2025).
- [20] X. Duan, J. Zhang, Z. Zhu, Y. Liu, Z. Zhang, I. Žutić, and T. Zhou, Antiferroelectric altermagnets: Antiferroelectricity alters magnets, *Phys. Rev. Lett.* **134**, 106801 (2025).
- [21] M. Gu, Y. Liu, H. Zhu, K. Yananose, X. Chen, Y. Hu, A. Stroppa, and Q. Liu, Ferroelectric switchable altermagnetism, *Phys. Rev. Lett.* **134**, 106802 (2025).
- [22] L. Yu, H. J. Zhao, L. Bellaïche, and Y. Ma, Electrically switchable nonrelativistic zeeman spin splittings in collinear antiferromagnets, *Phys. Rev. Lett.* **135**, 256704 (2025).
- [23] J.-X. Hu, O. Matsyshyn, and J. C. W. Song, Nonlinear superconducting magnetoelectric effect, *Phys. Rev. Lett.* **134**, 026001 (2025).
- [24] D. Zhu, Z.-Y. Zhuang, Z. Wu, and Z. Yan, Topological superconductivity in two-dimensional altermagnetic metals, *Phys. Rev. B* **108**, 184505 (2023).
- [25] S. Sumita, M. Naka, and H. Seo, Fulde-ferrell-larkin-ovchinnikov state induced by antiferromagnetic order in κ -type organic conductors, *Phys. Rev. Res.* **5**, 043171 (2023).
- [26] S.-B. Zhang, L.-H. Hu, and T. Neupert, Finite-momentum cooper pairing in proximitized altermagnets, *Nature Communications* **15**, 1801 (2024).
- [27] S. A. A. Ghorashi, T. L. Hughes, and J. Cano, Altermagnetic routes to majorana modes in zero net magnetization, *Phys. Rev. Lett.* **133**, 106601 (2024).
- [28] D. Chakraborty and A. M. Black-Schaffer, Zero-field finite-momentum and field-induced superconductivity in altermagnets, *Phys. Rev. B* **110**, L060508 (2024).
- [29] S. Hong, M. J. Park, and K.-M. Kim, Unconventional p -wave and finite-momentum superconductivity induced by altermagnetism through the formation of bogoliubov fermi surface, *Phys. Rev. B* **111**, 054501 (2025).
- [30] K. Mukasa and Y. Masaki, Finite-momentum superconductivity in two-dimensional altermagnets with a rashba-type spin-orbit coupling, *Journal of the Physical Society of Japan* **94**, 064705 (2025).
- [31] X.-J. Luo, Z.-T. Sun, X. Feng, M. Tian, and K. T. Law, *Hidden zeeman field in odd-parity magnets: An ideal platform for topological superconductivity* (2026), arXiv:2603.15147 [cond-mat.supr-con].
- [32] W. F. Brinkman and R. J. Elliott, Theory of spin-space groups, *Proceedings of the Royal Society of London. A. Mathematical and Physical Sciences* **294**, 343 (1966).
- [33] D. Litvin and W. Opechowski, Spin groups, *Physica* **76**, 538 (1974).
- [34] P. Liu, J. Li, J. Han, X. Wan, and Q. Liu, Spin-group symmetry in magnetic materials with negligible spin-orbit coupling, *Phys. Rev. X* **12**, 021016 (2022).
- [35] X. Chen, J. Ren, Y. Zhu, Y. Yu, A. Zhang, P. Liu, J. Li, Y. Liu, C. Li, and Q. Liu, Enumeration and representation theory of spin space groups, *Phys. Rev. X* **14**, 031038 (2024).
- [36] Y. Jiang, Z. Song, T. Zhu, Z. Fang, H. Weng, Z.-X. Liu, J. Yang, and C. Fang, Enumeration of spin-space groups: Toward a complete description of symmetries of magnetic orders, *Phys. Rev. X* **14**, 031039 (2024).
- [37] Z. Xiao, J. Zhao, Y. Li, R. Shindou, and Z.-D. Song, Spin space groups: Full classification and applications, *Phys. Rev. X* **14**, 031037 (2024).
- [38] X. Chen, Y. Liu, P. Liu, Y. Yu, J. Ren, J. Li, A. Zhang, and Q. Liu, Unconventional magnons in collinear magnets dictated by spin space groups, *Nature* **640**, 349 (2025).
- [39] X.-J. Luo, J.-X. Hu, M.-L. Hu, and K. T. Law, *Spin group symmetry criteria for odd-parity magnets* (2026), arXiv:2510.05512 [cond-mat.other].
- [40] X.-J. Luo, J.-X. Hu, M. Hu, and K. T. Law, *Spin group symmetry criteria for unconventional magnetism* (2026),

- arXiv:2603.07643 [cond-mat.str-el].
- [41] L. Šmejkal, R. González-Hernández, T. Jungwirth, and J. Sinova, Crystal time-reversal symmetry breaking and spontaneous hall effect in collinear antiferromagnets, *Science Advances* **6**, eaz8809 (2020).
- [42] Z. Feng, X. Zhou, L. Šmejkal, L. Wu, Z. Zhu, H. Guo, R. González-Hernández, X. Wang, H. Yan, P. Qin, X. Zhang, H. Wu, H. Chen, Z. Meng, L. Liu, Z. Xia, J. Sinova, T. Jungwirth, and Z. Liu, An anomalous hall effect in altermagnetic ruthenium dioxide, *Nature Electronics* **5**, 735 (2022).
- [43] X. Zhou, W. Feng, R.-W. Zhang, L. Šmejkal, J. Sinova, Y. Mokrousov, and Y. Yao, Crystal thermal transport in altermagnetic RuO₂, *Phys. Rev. Lett.* **132**, 056701 (2024).
- [44] O. Fedchenko, J. Minár, A. Akashdeep, S. W. D'Souza, D. Vasilyev, O. Tkach, L. Odenbreit, Q. Nguyen, D. Kutnyakhov, N. Wind, L. Wenthaus, M. Scholz, K. Rossnagel, M. Hoesch, M. Aeschlimann, B. Stadtmüller, M. Kläui, G. Schönhense, T. Jungwirth, A. B. Hellenes, G. Jakob, L. Šmejkal, J. Sinova, and H.-J. Elmers, Observation of time-reversal symmetry breaking in the band structure of altermagnetic RuO₂, *Science Advances* **10**, eadj4883 (2024).
- [45] Z. Lin, D. Chen, W. Lu, X. Liang, S. Feng, K. Yamagami, J. Osiecki, M. Leandersson, B. Thiagarajan, J. Liu, C. Felser, and J. Ma, Observation of giant spin splitting and d-wave spin texture in room temperature altermagnet RuO₂ (2024), arXiv:2402.04995 [cond-mat.mtrl-sci].
- [46] H. Chen, Z.-A. Wang, P. Qin, Z. Meng, X. Zhou, X. Wang, L. Liu, G. Zhao, Z. Duan, T. Zhang, J. Liu, D.-F. Shao, C. Jiang, and Z. Liu, Spin-splitting magnetoresistance in altermagnetic RuO₂ thin films, *Advanced Materials* **37**, 2507764 (2025).
- [47] Y.-C. Wang, Z.-Y. Shen, C.-H. Lin, W.-C. Hsu, Y.-S. Chen, Y.-Y. Chin, A. K. Singh, W.-L. Lee, C.-T. Chen, S.-Y. Huang, and D. Qu, Absence of transport altermagnetic spin-splitting effect in RuO₂, *Nano Letters* **26**, 2548 (2026).
- [48] B. Jiang, M. Hu, J. Bai, Z. Song, C. Mu, G. Qu, W. Li, W. Zhu, H. Pi, Z. Wei, Y.-J. Sun, Y. Huang, X. Zheng, Y. Peng, L. He, S. Li, J. Luo, Z. Li, G. Chen, H. Li, H. Weng, and T. Qian, A metallic room-temperature d-wave altermagnet, *Nature Physics* **21**, 754 (2025).
- [49] F. Zhang, X. Cheng, Z. Yin, C. Liu, L. Deng, Y. Qiao, Z. Shi, S. Zhang, J. Lin, Z. Liu, M. Ye, Y. Huang, X. Meng, C. Zhang, T. Okuda, K. Shimada, S. Cui, Y. Zhao, G.-H. Cao, S. Qiao, J. Liu, and C. Chen, Crystal-symmetry-paired spin-valley locking in a layered room-temperature metallic altermagnet candidate, *Nature Physics* **21**, 760 (2025).
- [50] C.-C. Liu, J. Li, J.-Y. Liu, J.-Y. Lu, H.-X. Li, Y. Liu, and G.-H. Cao, Physical properties and first-principles calculations of an altermagnet candidate Cs_{1- δ} V₂Te₂O, *Phys. Rev. B* **112**, 224439 (2025).
- [51] Z. Wang, S. Yu, X. Cheng, X. Xiao, W. Ma, F. Quan, H. Song, K. Zhang, Y. Zhang, Y. Ma, W. Liu, P. Yadav, X. Shi, Z. Wang, Q. Niu, Y. Gao, B. Xiang, J. Liu, Z. Wang, and X. Chen, Atomic-scale spin sensing of a 2D d-wave altermagnet via helical tunneling (2025), arXiv:2512.23290 [cond-mat.mes-hall].
- [52] G. Yang, C. Li, C. Wang, X. Zhao, Y. Wan, H. Gui, G. Zeng, S. Cao, C. Hu, D. Chen, Y. Liu, Y. Song, F. Liu, L.-H. Hu, L. Jiao, and H. Yuan, Visualizing spin-polarization of an altermagnet KV₂Se₂O via spin-selective tunneling (2026), arXiv:2603.21969 [cond-mat.mtrl-sci].
- [53] D. Fu, L. Yang, Y. Shen, K. Xiao, Y. Wang, W. Jiang, Z. Wang, Y. Yao, Q.-K. Xue, and W. Li, Atomic-scale visualization of d-wave altermagnetism (2026), arXiv:2512.24114 [cond-mat.mtrl-sci].
- [54] Y. Liu, C.-C. Xu, J.-K. Bao, B.-J. Lv, H. Li, J. Li, Y.-Q. Lin, H.-X. Li, Y.-M. Lu, X.-Y. Zhao, W.-Z. Yang, Z.-Y. Zhang, X.-Y. Chen, W.-H. Jiao, J.-Y. Liu, B.-R. Zhu, and G.-H. Cao, Altermagnetism and room-temperature metal-to-insulator transition in CsCr₂S₂O (2026), arXiv:2604.02114 [cond-mat.mtrl-sci].
- [55] J. Ding, Z. Jiang, X. Chen, Z. Tao, Z. Liu, T. Li, J. Liu, J. Sun, J. Cheng, J. Liu, Y. Yang, R. Zhang, L. Deng, W. Jing, Y. Huang, Y. Shi, M. Ye, S. Qiao, Y. Wang, Y. Guo, D. Feng, and D. Shen, Large band splitting in g-wave altermagnet CrSb, *Phys. Rev. Lett.* **133**, 206401 (2024).
- [56] M. Zeng, M.-Y. Zhu, Y.-P. Zhu, X.-R. Liu, X.-M. Ma, Y.-J. Hao, P. Liu, G. Qu, Y. Yang, Z. Jiang, K. Yamagami, M. Arita, X. Zhang, T.-H. Shao, Y. Dai, K. Shimada, Z. Liu, M. Ye, Y. Huang, Q. Liu, and C. Liu, Observation of spin splitting in room-temperature metallic antiferromagnet CrSb, *Advanced Science* **11**, 2406529 (2024).
- [57] S. Reimers, L. Odenbreit, L. Šmejkal, V. N. Strocov, P. Constantinou, A. B. Hellenes, R. Jaeschke Ubiergo, W. H. Campos, V. K. Bharadwaj, A. Chakraborty, T. Denneulin, W. Shi, R. E. Dunin-Borkowski, S. Das, M. Kläui, J. Sinova, and M. Jourdan, Direct observation of altermagnetic band splitting in CrSb thin films, *Nature Communications* **15**, 2116 (2024).
- [58] G. Yang, Z. Li, S. Yang, J. Li, H. Zheng, W. Zhu, Z. Pan, Y. Xu, S. Cao, W. Zhao, A. Jana, J. Zhang, M. Ye, Y. Song, L.-H. Hu, L. Yang, J. Fujii, I. Vobornik, M. Shi, H. Yuan, Y. Zhang, Y. Xu, and Y. Liu, Three-dimensional mapping of the altermagnetic spin splitting in CrSb, *Nature Communications* **16**, 1442 (2025).
- [59] W. Lu, S. Feng, Y. Wang, D. Chen, Z. Lin, X. Liang, S. Liu, W. Feng, K. Yamagami, J. Liu, C. Felser, Q. Wu, and J. Ma, Signature of topological surface bands in altermagnetic weyl semimetal CrSb, *Nano Letters* **25**, 7343 (2025).
- [60] S. Lee, S. Lee, S. Jung, J. Jung, D. Kim, Y. Lee, B. Seok, J. Kim, B. G. Park, L. Šmejkal, C.-J. Kang, and C. Kim, Broken kramers degeneracy in altermagnetic MnTe, *Phys. Rev. Lett.* **132**, 036702 (2024).
- [61] J. Krempaský, L. Šmejkal, S. W. D'Souza, M. Hajlaoui, G. Springholz, K. Uhlířová, F. Alarab, P. C. Constantinou, V. Strocov, D. Usanov, W. R. Pudelko, R. González-Hernández, A. Birk Hellenes, Z. Jansa, H. Reichlová, Z. Šobáň, R. D. Gonzalez Betancourt, P. Wadley, J. Sinova, D. Kriegner, J. Minár, J. H. Dil, and T. Jungwirth, Altermagnetic lifting of kramers spin degeneracy, *Nature* **626**, 517 (2024).
- [62] T. Osumi, S. Souma, T. Aoyama, K. Yamauchi, A. Honma, K. Nakayama, T. Takahashi, K. Ohgushi, and T. Sato, Observation of a giant band splitting in altermagnetic MnTe, *Phys. Rev. B* **109**, 115102 (2024).
- [63] M. Hajlaoui, S. Wilfred D'Souza, L. Šmejkal, D. Kriegner, G. Krizman, T. Zakusylo, N. Olszowska, O. Caha, J. Michalička, J. Sánchez-Barriga, A. Marmodoro,

- K. Vyborny, A. Ernst, M. Cinchetti, J. Minar, T. Jungwirth, and G. Springholz, Temperature dependence of relativistic valence band splitting induced by an altermagnetic phase transition, *Advanced Materials* **36**, 2314076 (2024).
- [64] M. Chilcote, A. R. Mazza, Q. Lu, I. Gray, Q. Tian, Q. Deng, D. Moseley, A.-H. Chen, J. Lapano, J. S. Gardner, G. Eres, T. Z. Ward, E. Feng, H. Cao, V. Lauter, M. A. McGuire, R. Hermann, D. Parker, M.-G. Han, A. Kayani, G. Rimal, L. Wu, T. R. Charlton, R. G. Moore, and M. Brahlek, Stoichiometry-induced ferromagnetism in altermagnetic candidate MnTe, *Advanced Functional Materials* **34**, 2405829 (2024).
- [65] O. J. Amin, A. Dal Din, E. Golias, Y. Niu, A. Zakharov, S. C. Fromage, C. J. B. Fields, S. L. Heywood, R. B. Cousins, F. Maccherozzi, J. Krempasky, J. H. Dil, D. Kriegner, B. Kiraly, R. P. Champion, A. W. Rushforth, K. W. Edmonds, S. S. Dhesi, L. Šmejkal, T. Jungwirth, and P. Wadley, Nanoscale imaging and control of altermagnetism in MnTe, *Nature* **636**, 348 (2024).
- [66] A. B. Hellenes, T. Jungwirth, R. Jaeschke-Ubiergo, A. Chakraborty, J. Sinova, and L. Šmejkal, *P-wave magnets* (2024), [arXiv:2309.01607 \[cond-mat.mes-hall\]](https://arxiv.org/abs/2309.01607).
- [67] B. Brekke, P. Sukhachov, H. G. Giil, A. Brataas, and J. Linder, Minimal models and transport properties of unconventional *p*-wave magnets, *Phys. Rev. Lett.* **133**, 236703 (2024).
- [68] J. Mitscherling, J. Priessnitz, C. K. Geschner, and L. Šmejkal, Microscopic origin of *p*-wave magnetism (2026), [arXiv:2603.09736 \[cond-mat.mes-hall\]](https://arxiv.org/abs/2603.09736).
- [69] M. Ezawa, Purely electrical detection of the spin-splitting vector in *p*-wave magnets based on linear and nonlinear conductivities, *Phys. Rev. B* **112**, 125412 (2025).
- [70] A. Chakraborty, A. Birk Hellenes, R. Jaeschke-Ubiergo, T. Jungwirth, L. Šmejkal, and J. Sinova, Highly efficient non-relativistic edelstein effect in nodal *p*-wave magnets, *Nature Communications* **16**, 7270 (2025).
- [71] N. A. A. Pari, R. Jaeschke-Ubiergo, A. Chakraborty, L. Šmejkal, and J. Sinova, Nonrelativistic linear edelstein effect in helical EuIn_2As_2 , *Phys. Rev. B* **112**, 024404 (2025).
- [72] P. Sukhachov, H. G. Giil, B. Brekke, and J. Linder, Coexistence of *p*-wave magnetism and superconductivity, *Phys. Rev. B* **111**, L220403 (2025).
- [73] Y. Fukaya, B. Lu, K. Yada, Y. Tanaka, and J. Cayao, Superconducting phenomena in systems with unconventional magnets, *Journal of Physics: Condensed Matter* **37**, 313003 (2025).
- [74] M. Khodas, L. Šmejkal, and I. I. Mazin, Nonrelativistic-ising superconductivity in *p*-wave magnets (2026), [arXiv:2601.19829 \[cond-mat.supr-con\]](https://arxiv.org/abs/2601.19829).
- [75] Z.-T. Sun, X. Feng, Y.-M. Xie, B. T. Zhou, J.-X. Hu, and K. T. Law, Pseudo-ising superconductivity induced by *p*-wave magnetism, *Phys. Rev. B* **112**, 214504 (2025).
- [76] K. Maeda, B. Lu, K. Yada, and Y. Tanaka, Theory of tunneling spectroscopy in unconventional *p*-wave magnet-superconductor hybrid structures, *Journal of the Physical Society of Japan* **93**, 114703 (2024).
- [77] K.-M. Kim, G. Sim, and M. J. Park, Topological ising superconductivity in two-dimensional *p*-wave magnet (2026), [arXiv:2605.01686 \[cond-mat.str-el\]](https://arxiv.org/abs/2605.01686).
- [78] A. Pal, P. Dutta, and A. Saha, Emergent superconducting phases in unconventional *p*-wave magnets: Topological superconductivity, bogoliubov fermi surfaces and superconducting diode effect (2026), [arXiv:2603.03221 \[cond-mat.supr-con\]](https://arxiv.org/abs/2603.03221).
- [79] Y. Yu, M. B. Lyngby, T. Shishidou, M. Roig, A. Kreisel, M. Weinert, B. M. Andersen, and D. F. Agterberg, Odd-parity magnetism driven by antiferromagnetic exchange, *Phys. Rev. Lett.* **135**, 046701 (2025).
- [80] Q. Song, S. Stavrić, P. Barone, A. Droghetti, D. S. Antonenko, J. W. F. Venderbos, C. A. Occhialini, B. Ilyas, E. Ergeçen, N. Gedik, S.-W. Cheong, R. M. Fernandes, S. Picozzi, and R. Comin, Electrical switching of a *p*-wave magnet, *Nature* **642**, 64 (2025).
- [81] R. Yamada, M. T. Birch, P. R. Baral, S. Okumura, R. Nakano, S. Gao, M. Ezawa, T. Nomoto, J. Masell, Y. Ishihara, K. K. Kolincio, I. Belopolski, H. Sagayama, H. Nakao, K. Ohishi, T. Ohhara, R. Kiyonagi, T. Nakajima, Y. Tokura, T.-h. Arima, Y. Motome, M. M. Hirschmann, and M. Hirschberger, A metallic *p*-wave magnet with commensurate spin helix, *Nature* **646**, 837 (2025).
- [82] R. Dsouza, A. Kreisel, B. M. Andersen, D. F. Agterberg, and M. H. Christensen, Odd-parity magnetism in *fe*-based superconductors with coplanar magnetic order, *Phys. Rev. B* **113**, 144509 (2026).
- [83] S. Hayami, Y. Yanagi, and H. Kusunose, Bottom-up design of spin-split and reshaped electronic band structures in antiferromagnets without spin-orbit coupling: Procedure on the basis of augmented multipoles, *Phys. Rev. B* **102**, 144441 (2020).
- [84] M. M. Hirschmann, A. Furusaki, and M. Hirschberger, *Symmetry-enforced nodal f-wave magnets* (2026), [arXiv:2603.17406 \[cond-mat.mes-hall\]](https://arxiv.org/abs/2603.17406).
- [85] S. Lv, Y. Meng, and H. Zou, *Spontaneous parity breaking in quantum antiferromagnets on the triangular lattice* (2026), [arXiv:2602.05901 \[cond-mat.str-el\]](https://arxiv.org/abs/2602.05901).
- [86] L. M. Corliss, N. Elliott, J. M. Hastings, and R. L. Sass, Magnetic structure of chromium selenide, *Phys. Rev.* **122**, 1402 (1961).
- [87] S. Xu, M. Yang, Y. Li, B. Shen, S. Gong, J. Huang, P. Yu, Y. Li, and J. Luo, Spin symmetry study in non-collinear CrSe: Odd-wave magnetism induced by glide mirror symmetry breaking, *Applied Physics Letters* **127**, 032407 (2025).
- [88] Y. Yang, P. Guo, S. Liu, Y. Wu, C. Li, H. Yan, Y. Cao, Y. Lu, and Y. Luo, Toward an understanding of magnetism in the strained 1T-MnCl_2 : The 90° super-exchange and *d*-*p* hybridization, *Computational Materials Science* **250**, 113726 (2025).
- [89] See Supporting Information at [url] for: (1) Computational details, The Supplementary Materials include Refs..
- [90] Y. Yu, X. Chen, Y. Zhu, Y. Li, R. Xiong, J. Li, Y. Liu, and Q. Liu, *Identifying oriented spin space groups and related physical properties using an online platform findspingroup* (2026), [arXiv:2604.21397 \[cond-mat.mtrl-sci\]](https://arxiv.org/abs/2604.21397).
- [91] A. I. Snow, Neutron diffraction investigation of the atomic magnetic moment orientation in the antiferromagnetic compound CrSb, *Phys. Rev.* **85**, 365 (1952).
- [92] W. J. Takei, D. E. Cox, and G. Shirane, Magnetic structures in the MnSb-CrSb system, *Phys. Rev.* **129**, 2008 (1963).
- [93] S. Polesya, G. Kuhn, S. Mankovsky, H. Ebert, M. Regus, and W. Bensch, Structural and magnetic properties of

- CrSb compounds: NiAs structure, *Journal of Physics: Condensed Matter* **24**, 036004 (2011).
- [94] Masrouj, Rachid, Hlil, El Kebir, Hamedoun, Mohamed, and Benyoussef, Abdelilah, Electronic and magnetic structures of CrSb compounds investigated by first principles, mean field and series expansion calculations, *Eur. Phys. J. Appl. Phys.* **67**, 21101 (2014).
- [95] S. Rooj, J. Chakraborty, and N. Ganguli, Hexagonal MnTe with antiferromagnetic spin splitting and hidden rashba-dresselhaus interaction for antiferromagnetic spintronics, *Advanced Physics Research* **3**, 2300050 (2024).
- [96] D. Kriegner, H. Reichlova, J. Grenzer, W. Schmidt, E. Ressouche, J. Godinho, T. Wagner, S. Y. Martin, A. B. Shick, V. V. Volobuev, G. Springholz, V. Holý, J. Wunderlich, T. Jungwirth, and K. Vyborny, Magnetic anisotropy in antiferromagnetic hexagonal MnTe, *Phys. Rev. B* **96**, 214418 (2017).
- [97] V. P. Kravchuk, K. V. Yershov, J. I. Facio, Y. Guo, O. Janson, O. Gomonay, J. Sinova, and J. van den Brink, Chiral magnetic excitations and domain textures of g -wave altermagnets, *Phys. Rev. B* **112**, 144421 (2025).
- [98] I. I. Mazin, Altermagnetism in mnte: Origin, predicted manifestations, and routes to detwinning, *Phys. Rev. B* **107**, L100418 (2023).
- [99] M. Chevreton, M. Murat, C. Eyraud, and E. Bertaut, Structure et conductibilité électrique des composés à lacunes ordonnées du système chrome-sélénium, *Journal de Physique* **24**, 443 (1963).
- [100] Y. Adachi, M. Ohashi, T. Kaneko, M. Yuzuri, Y. Yamaguchi, S. Funahashi, and Y. Morii, Magnetic structure of rhombohedral Cr₂Se₃, *Journal of the Physical Society of Japan* **63**, 1548 (1994).
- [101] M. Yuzuri, Magnetic properties of the compound Cr-Se system, *Journal of the Physical Society of Japan* **35**, 1252 (1973).
- [102] M. Yuzuri and K. Segi, Magnetic properties of the Cr₂Se_{3-x}Te_x ($x = 0 \sim 3$) and Cr₃Se_{4-x}Te_x ($x = 0 \sim 4$) systems, *Physica B+C* **86-88**, 891 (1977).
- [103] J. Yan, X. Luo, F. C. Chen, Q. L. Pei, G. T. Lin, Y. Y. Han, L. Hu, P. Tong, W. H. Song, X. B. Zhu, and Y. P. Sun, Anomalous hall effect in two-dimensional non-collinear antiferromagnetic semiconductor Cr_{0.68}Se, *Applied Physics Letters* **111**, 022401 (2017).
- [104] M. Liu, Y. L. Huang, J. Gou, Q. Liang, R. Chua, Aramel, S. Duan, L. Zhang, L. Cai, X. Yu, D. Zhong, W. Zhang, and A. T. S. Wee, Diverse structures and magnetic properties in nonlayered monolayer chromium selenide, *The Journal of Physical Chemistry Letters* **12**, 7752 (2021).
- [105] A. Roy, R. Dey, T. Pramanik, A. Rai, R. Schalip, S. Majumder, S. Guchhait, and S. K. Banerjee, Structural and magnetic properties of molecular beam epitaxy grown chromium selenide thin films, *Phys. Rev. Mater.* **4**, 025001 (2020).
- [106] A. S. M. Aljaloud, A. F. Qasrawi, and L. H. K. Alfheid, Effects of pb nanosheets substrates on the optical and electrical properties CrSe thin films, *Physica Scripta* **98**, 115950 (2023).
- [107] Y. Wu, G. Yin, L. Pan, A. J. Grutter, Q. Pan, A. Lee, D. A. Gilbert, J. A. Borchers, W. Ratcliff, A. Li, X.-d. Han, and K. L. Wang, Large exchange splitting in monolayer graphene magnetized by an antiferromagnet, *Nature Electronics* **3**, 604 (2020).
- [108] D. Sofronov, I. Pritula, S. Naydenov, O. Kapustnyk, O. Lukienko, and P. Mateychenko, *Synthesis of chromium, cobalt and iron monoselenides as high-purity precursors for doped optical crystal growth*, Research Square (2026).
- [109] T. Hirone and S. Chiba, On the magnetic anisotropy of single crystal of chromium telluride, *Journal of the Physical Society of Japan* **15**, 991 (1960).
- [110] M. Wang, L. Kang, J. Su, L. Zhang, H. Dai, H. Cheng, X. Han, T. Zhai, Z. Liu, and J. Han, Two-dimensional ferromagnetism in CrTe flakes down to atomically thin layers, *Nanoscale* **12**, 16427 (2020).
- [111] L. Kang, C. Ye, X. Zhao, X. Zhou, J. Hu, Q. Li, D. Liu, C. M. Das, J. Yang, D. Hu, J. Chen, X. Cao, Y. Zhang, M. Xu, J. Di, D. Tian, P. Song, G. Kutty, Q. Zeng, Q. Fu, Y. Deng, J. Zhou, A. Ariando, F. Miao, G. Hong, Y. Huang, S. J. Pennycook, K.-T. Yong, W. Ji, X. Renshaw Wang, and Z. Liu, Phase-controllable growth of ultrathin 2D magnetic FeTe crystals, *Nature Communications* **11**, 3729 (2020).
- [112] X.-J. Luo, D. Li, R.-C. Xiao, D.-F. Shao, L. Li, M. Tian, and Y. Yao, Unconventional magnetism: Symmetry classification, hybrid-parity and unconstrained-parity classes (2026), [arXiv:2605.21336v1 \[cond-mat.mtrl-sci\]](https://arxiv.org/abs/2605.21336v1).
- [113] Z.-Y. Zhuang, J.-X. Hu, S.-B. Zhang, L.-H. Hu, and Z. Yan, Mixed-parity altermagnetism in collinear spin-orbital magnets (2026), [arXiv:2605.05205 \[cond-mat.mes-hall\]](https://arxiv.org/abs/2605.05205).

Supplementary Materials for “Global magnetic phase diagram and multiple unconventional magnets in NiAs-type compounds”

Shibo Shen^{1,2,3} and Yilin Wang^{1,2,3,*}

¹*School of Emerging Technology, University of Science and Technology of China, Hefei 230026, China*

²*Hefei National Laboratory, University of Science and Technology of China, Hefei 230088, China*

³*New Cornerstone Science Laboratory, University of Science and Technology of China, Hefei, 230026, China*

(Dated: May 28, 2026)

S-I. Computational Details

Density functional theory (DFT) calculations are performed using the projector augmented wave (PAW) [1] method as implemented in the Vienna *Ab-initio* Simulation Package (VASP) [2]. The exchange-correlation functional of generalized gradient approximation (GGA-PBE) is used. The cutoff of plane-wave energy is 500 eV. Γ -centered K-point grid of $16 \times 16 \times 8$, $10 \times 10 \times 8$, $8 \times 16 \times 8$ and $8 \times 6 \times 8$ are used for the $1 \times 1 \times 1$, $\sqrt{3} \times \sqrt{3} \times 1$, $2 \times 1 \times 1$, and $2 \times 3 \times 1$ supercells, respectively. The Se-doping is simulated using the method of virtual crystal approximation (VCA) [3]. The spin-orbital coupling is not considered in the calculations. The 2D Fermi surfaces are visualized and analyzed with Pyprocar [4, 5].

We use experimental lattice constants for CrSb, MnTe, and CrSe. For FeTe and CrTe, we perform full structural relaxation for all magnetic configurations. This is because these materials lie near the phase boundary, where the magnetic ground state is very sensitive to lattice constants and atomic positions. For structural relaxation, the criteria for forces convergence is less than 0.005 eV/Å. The magnetic structures of Stripe-1/Stripe-2 and Zigzag-1/Zigzag-2 are shown in Fig. S1.

The magnetic exchange couplings J_i are calculated based on the total energy difference method, with the help of the open-source OstravaJ code [6]. To calculate J_1 , J_2 and J_3 , we employ a $2\sqrt{3} \times \sqrt{3} \times 1$ supercell with a Γ -centered $5 \times 10 \times 8$ k-point grid. For CrSb, MnTe, CrSe, the experimental crystal structures are used. For CrTe, CrTe_{0.8}Se_{0.2} and FeTe, the relaxed crystal structures of the ground states are used. The lattice constants used for calculating J_i and the Cr-Cr distances for J_1 , J_2 , J_3 are listed in Table. S1. We use the convention that the spin vectors \vec{S}_i are normalized to 1, so that the parameters J_i are in units of energy.

S-II. Total Energies Formula Considering the Intralayer NNN Coupling J_4

As shown in Fig. S1(a), we consider the intralayer NNN coupling J_4 . The formula of total energy are,

$$E_{g\text{-AM1}} = -2J_1 + 6J_2 - 12J_3 + 6J_4, \quad (\text{S1})$$

$$E_{g\text{-AM2}} = -2J_1 - 2J_2 + 4J_3 + 6J_4, \quad (\text{S2})$$

$$E_{\text{Stripe-1}} = -2J_1 - 2J_2 + 4J_3 - 2J_4, \quad (\text{S3})$$

$$E_{\text{Zigzag-1}} = -2J_1 - 2J_2 + 4J_3 + \frac{2}{3}J_4, \quad (\text{S4})$$

$$E_{f\text{-OPM1}} = -2J_1 - 3J_2 + 6J_3 + 6J_4, \quad (\text{S5})$$

$$E_{f\text{-OPM2}} = 2J_1 - 3J_2 - 6J_3 + 6J_4. \quad (\text{S6})$$

$$E_{\text{FM}} = 2J_1 + 6J_2 + 12J_3 + 6J_4, \quad (\text{S7})$$

$$E_{\text{Stripe-2}} = 2J_1 - 2J_2 - 4J_3 - 2J_4. \quad (\text{S8})$$

$$E_{\text{Zigzag-2}} = 2J_1 - 2J_2 - 4J_3 + \frac{2}{3}J_4. \quad (\text{S9})$$

Based on Eqs. S1-S9, we obtain the critical condition for the Stripe-1, Zigzag-1, Stripe-2, and Zigzag-2 states to become ground states as follows,

* yilinwang@ustc.edu.cn

$$\text{Stripe-1} : J_1 > 0 \quad \text{and} \quad -J_4 < J_2 - 2J_3 < 8J_4, \quad (\text{S10})$$

$$\text{Zigzag-1} : J_1 > 0 \quad \text{and} \quad -\frac{2}{3}J_4 < J_2 - 2J_3 < \frac{16}{3}J_4, \quad (\text{S11})$$

$$\text{Stripe-2} : J_1 < 0 \quad \text{and} \quad -J_4 < J_2 + 2J_3 < 8J_4, \quad (\text{S12})$$

$$\text{Zigzag-2} : J_1 < 0 \quad \text{and} \quad -\frac{2}{3}J_4 < J_2 + 2J_3 < \frac{16}{3}J_4. \quad (\text{S13})$$

TABLE S1. The lattice constants and the Cr-Cr distances for the exchange couplings J_1 to J_4 of NiAs-type materials.

System	a (Å)	c (Å)	J_1 (Å)	J_2 (Å)	J_3 (Å)	J_4 (Å)
CrSb[7]	4.108	5.440	2.720	4.108	4.927	7.115
MnTe[8]	4.110	6.700	3.350	4.110	5.302	7.119
CrSe[9]	3.684	6.019	3.010	3.684	4.757	6.381
CrTe ^a	4.129	6.295	3.147	4.129	5.192	7.152
CrTe _{0.8} Se _{0.2} ^a	4.068	6.216	3.108	4.068	5.120	7.046
FeTe ^a	4.142	5.092	2.546	4.142	4.862	7.175
FeTe(a=0.97a ₀) ^a	4.018	5.092	2.546	4.018	4.757	6.960

^a Lattice constants obtained from DFT relaxation.

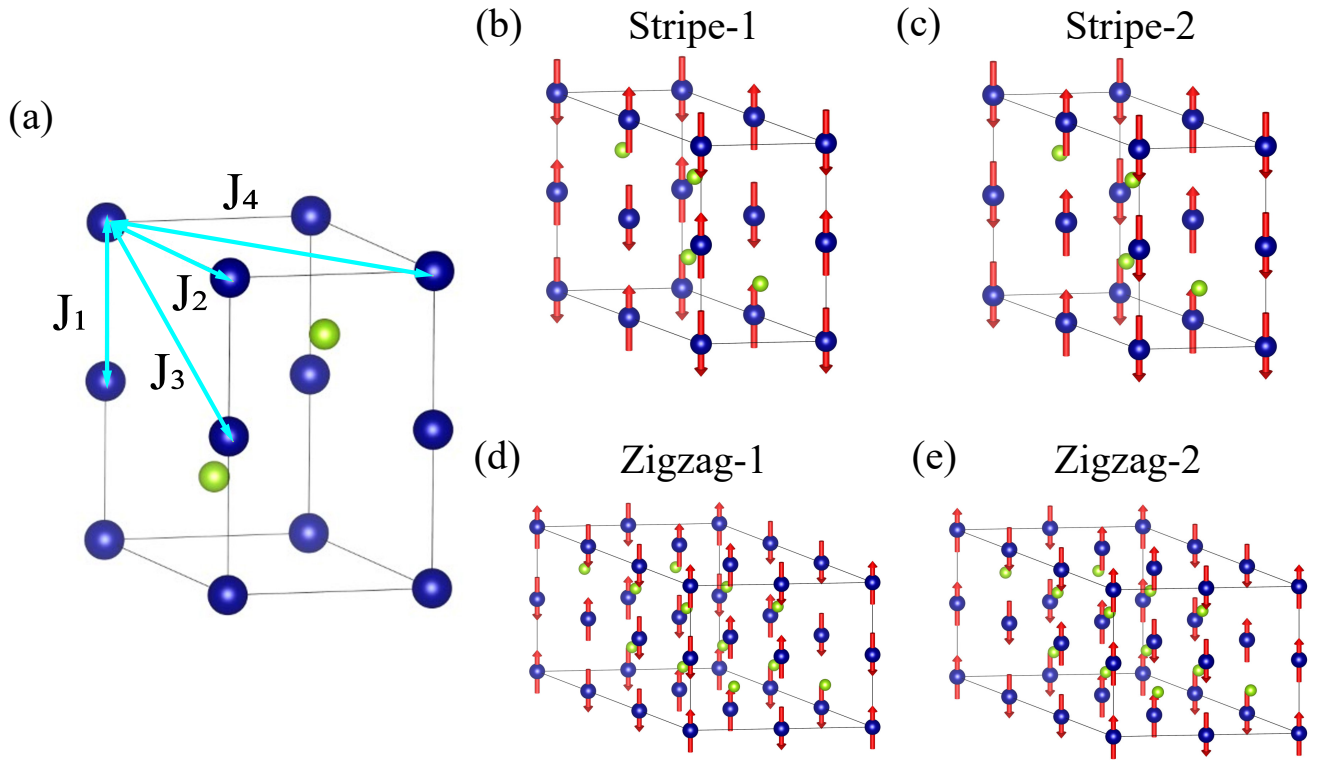


FIG. S1. (a) Definition of the exchange interactions J_1 - J_4 for the NiAs-type structure. (b)-(e) Magnetic structures of four conventional AFM orders.

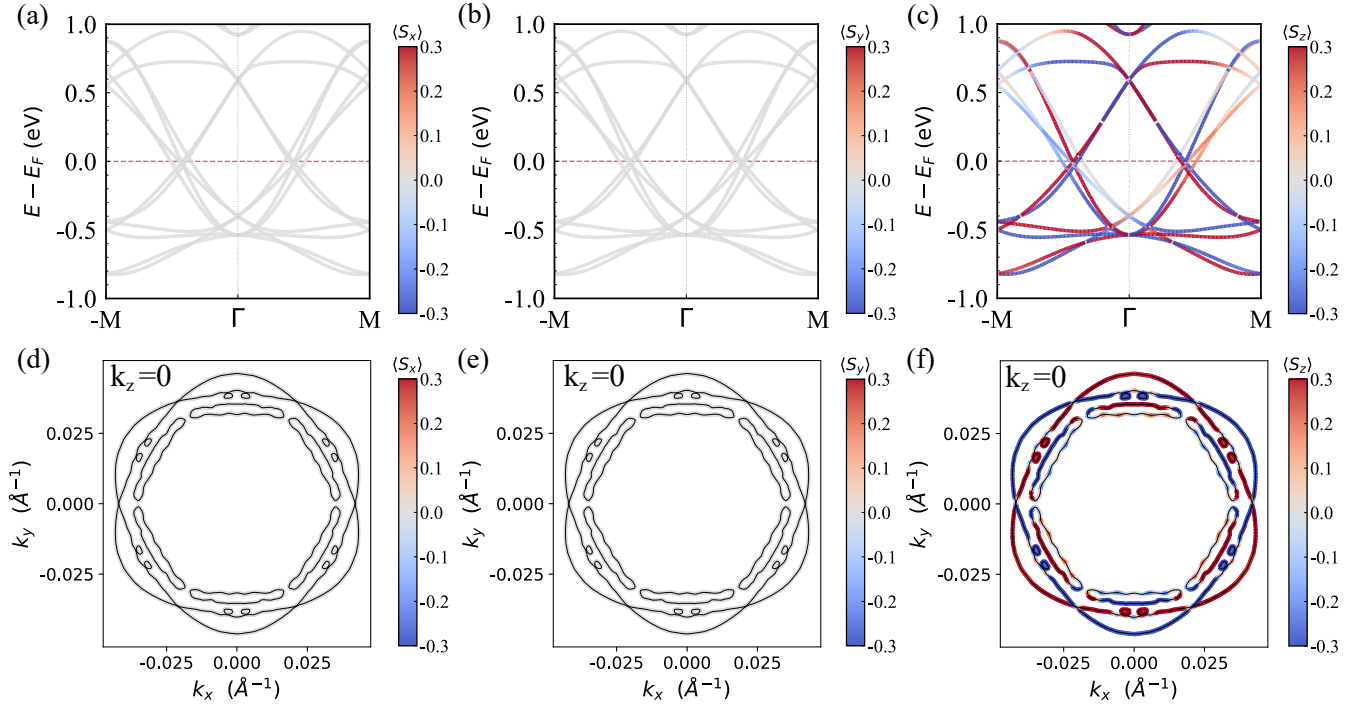


FIG. S2. Band structures and Fermi surface of CrSe in the f -OPM1 state. It demonstrates that $s_z(\mathbf{k}) = -s_z(-\mathbf{k})$, $s_{x,y}(\mathbf{k}) = 0$.

-
- [1] P. E. Blöchl, Projector augmented-wave method, *Phys. Rev. B* **50**, 17953 (1994).
 - [2] G. Kresse and J. Furthmüller, Efficient iterative schemes for ab initio total-energy calculations using a plane-wave basis set, *Phys. Rev. B* **54**, 11169 (1996).
 - [3] L. Bellaïche and D. Vanderbilt, Virtual crystal approximation revisited: Application to dielectric and piezoelectric properties of perovskites, *Phys. Rev. B* **61**, 7877 (2000).
 - [4] U. Herath, P. Tavazde, X. He, E. Bousquet, S. Singh, F. Muñoz, and A. H. Romero, Pyprocar: A python library for electronic structure pre/post-processing, *Computer Physics Communications* **251**, 107080 (2020).
 - [5] L. Lang, P. Tavazde, A. Tellez, E. Bousquet, H. Xu, F. Muñoz, N. Vasquez, U. Herath, and A. H. Romero, Expanding pyprocar for new features, maintainability, and reliability, *Computer Physics Communications* **297**, 109063 (2024).
 - [6] J. Priessnitz and D. Legut, *Ostravaj: a tool for calculating magnetic exchange interactions via dft* (2025), arXiv:2501.08251 [cond-mat.mtrl-sci].
 - [7] B. T. M. Willis, Crystal structure and antiferromagnetism of CrSb, *Acta Crystallographica* **6**, 425 (1953).
 - [8] S. Onari, T. Arai, and K. Kudo, Temperature dependence of the infrared absorption spectrum of antiferromagnetic semiconductor mnte, *Solid State Communications* **14**, 507 (1974).
 - [9] X. Oudet, Structures cristallines et liaisons, *Annales de Chimie* **8**, 483 (1983).

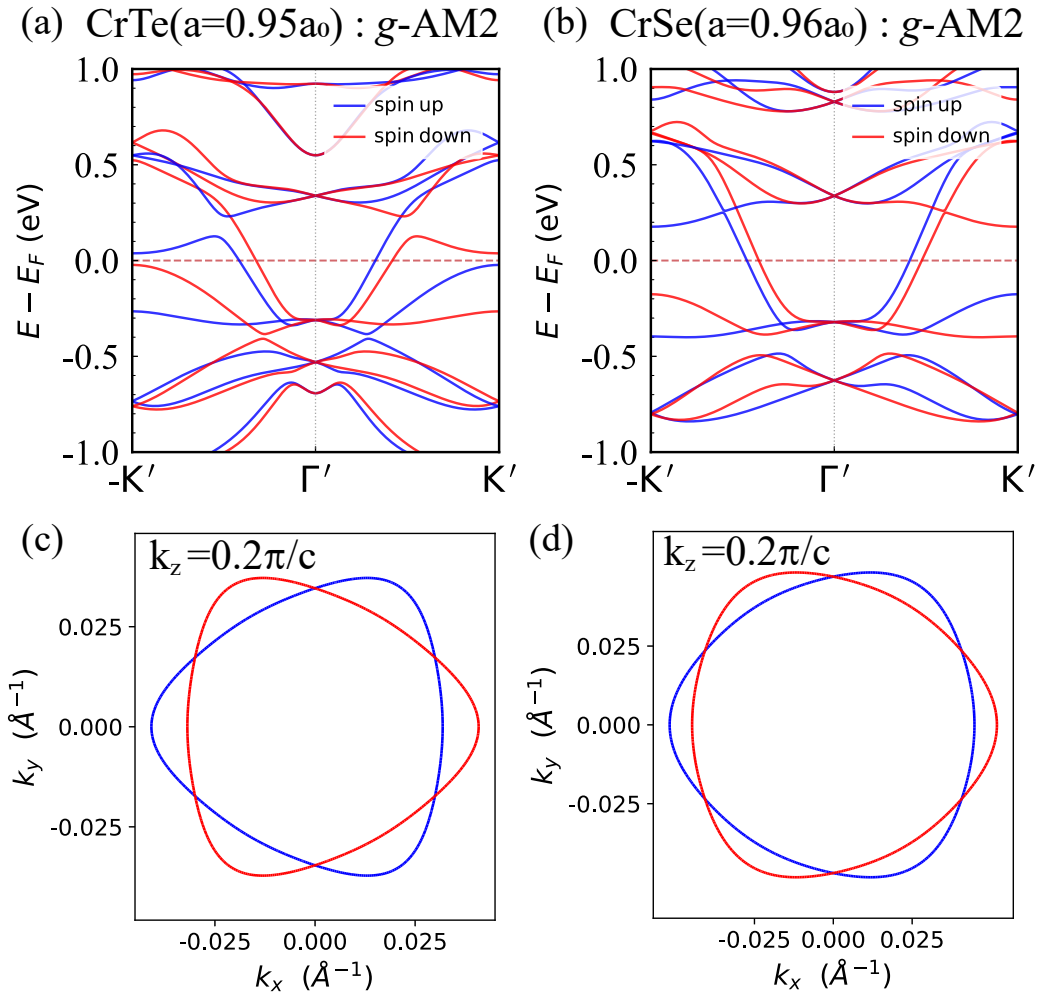


FIG. S3. Band structure and Fermi surface of CrTe ($a=0.95a_0$) and CrSe ($a=0.96a_0$) in the g -AM2 phase: (a),(b) Band structure along $-K'-\Gamma'-K'$. (c),(d) Fermi surface at $k_z = 0.2\pi/c$. Blue and red lines correspond to spin-up and spin-down states.

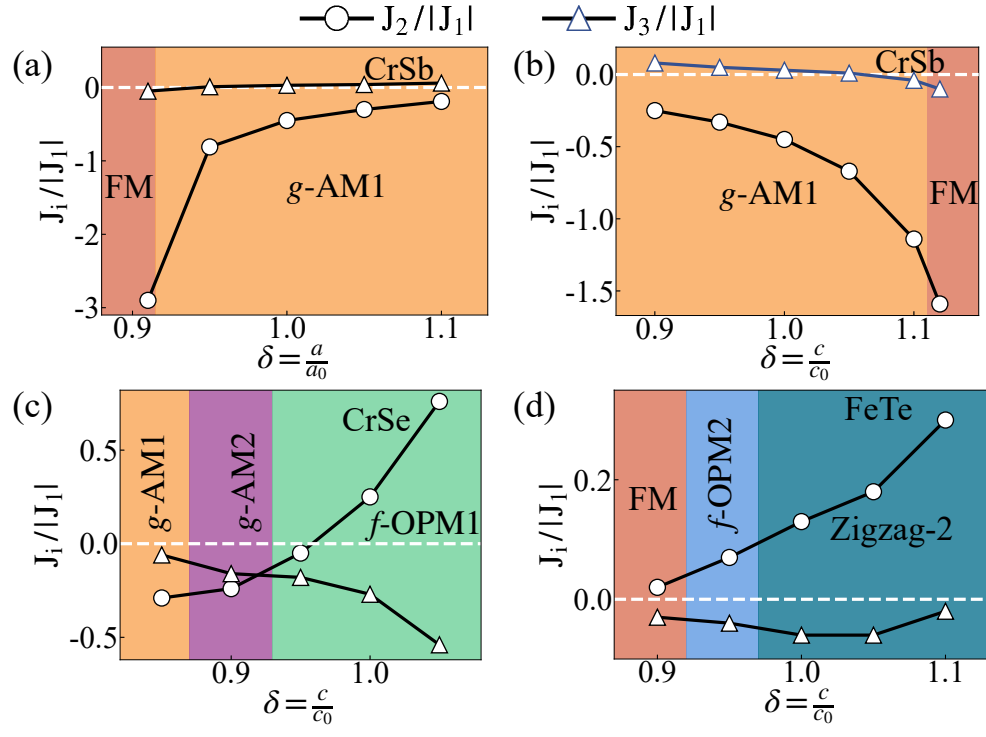


FIG. S4. DFT calculated $J_2/|J_1|$, $J_3/|J_1|$ and phase transitions of CrSb, CrSe and FeTe as changing lattice parameters a or c .